

DENSITY EFFECTS ON Mg II EMISSION LINES OF MIRA AB

M. R. SANAD¹, M. BOBROWSKY², M. A. HAMDY¹, AND M. S. ABO ELAZM¹

¹ National Research Institute of Astronomy and Geophysics, Astronomy Department, Helwan, Cairo P.O. Box 11421, Egypt; mrsanad1@yahoo.com

² Department of Physics, University of Maryland, College Park, MD 20742, USA; matt@mailaps.org

Received 2007 May 22; accepted 2008 October 15; published 2009 February 12

ABSTRACT

We present ultraviolet spectra of the Mira AB binary system taken by the *International Ultraviolet Explorer* during the period from 1979 to 1995. In this study, we concentrated on the Mg II *k* and *h* emission lines arising primarily from Mira B. The broad Mg II profiles from Mira B are enhanced on the red side of the profile and obscured on the blue side due to obscuration by the wind of Mira B. Small-scale variations in the flux of these lines are seen in these spectra. At some phases, the absorption and emission components appear in the blue side of the *k* and *h* lines and disappear at other phases. These components are not mentioned in previous studies. The absorption component originates from the circumstellar envelope, while the emission features likely arise from both Mira A and the accretion disk around Mira B. Overlying wind absorption is present on the red side of the Mg II lines, and this absorption extends out to -450 km s^{-1} . There is a relation between the parameters of these lines (line flux, line width, line velocity) and phase, which we attribute to an increase and decrease of the density of matter around Mira B at different times. Mg II emission in single Mira variables often displays a stronger *h* line than *k* line, opposite to the values of their oscillator strengths, resulting from circumstellar absorption from neutral metals over the *k* line. Meanwhile, non-Mira red giant stars typically show the *k* line being stronger than the *h* line in accordance with their respective oscillator strengths. The Mg II *k* to *h* emission from Mira B more closely follows the relative strength of *k* and *h* as seen in the non-Mira red giants than in the single Mira-type red giants.

Key words: accretion, accretion disks – binaries: general – circumstellar matter – stars: individual (Mira) – stars: variables: other – ultraviolet: stars

Online-only material: color figures

1. INTRODUCTION

Most stars at some point in their lives go through an unstable phase that leads to pulsation. There are many classes of these pulsating stars, among them are the Mira variables, with Mira A representing the prototype of the Mira variable stars. These stars are red giants on the Asymptotic Giant Branch (AGB). The distance to Mira AB is 128 pc according to *Hipparcos* (Perryman et al. 1997).

Mira A has a hot companion star, Mira B, with a separation of 0.4 (Figure 1). This star is assumed to be a white dwarf, although Jura & Helfand (1984) argued that the dearth of X-rays from the Mira system suggests that the companion is more likely a low-mass main-sequence star. Yamashita & Maehara (1977) described the optical spectrum of Mira B. Also, there are photometric observations by Warner (1972), who found substantial brightness variations on a time scale of hours. This confirms old visual observation of night-to-night variations by 1 mag (Joy 1954). Mira A ejects much of its mass in the form of a stellar wind, and some of this material is captured gravitationally by Mira B. The circumstellar shell of Mira A was seen in the line of sight (LOS) of Mira B by Deuch (1960) and Yamashita & Maehara (1978) in sharp Ca II *h* and *k* lines, and has been observed through circumstellar dust through OH, SiO maser emission (Sutton et al. 1978), and circumstellar CO emission (Wannier et al. 1980). Reimers & Cassatella (1985) analyzed some observations taken in the period from 1979 to 1983. Karovska et al. (1997) resolved the components of this binary system at UV and optical wavelengths using the *Hubble Space Telescope* (*HST*) Faint Object Camera (FOC) images and obtained the first spatially resolved spectrum of each star individually. The ultraviolet spectral regime showed many UV emission lines; among them are Mg II *k* and *h* lines. The Mg II

fluxes for single Mira variables peak around phase 0.3–0.45 and then decrease until becoming undetectable at about a phase of 0.7 (Brugel et al. 1986, Luttermoser 1996). While Mg II *k* and *h* are always present in Mira B, they do vary in flux through different visible light curve phases of Mira A. In this paper, we present all the observations taken by *International Ultraviolet Explorer* (*IUE*) for Mira AB through the period from 1979 to 1995 in order to study the nature of Mg II *k* and *h* emission lines, the variations of their profiles at different phases, the implications from their plots in velocity units, the correlations between their physical parameters (line flux, line width, line velocity) with phase, and how these parameters are affected by the density of matter as a result of the changing rate of accretion during the contraction and expansion of Mira A. Mg II emission in single Mira variables often displays a stronger *h* line than *k* line (Bookbinder et al. 1989), opposite to the values of their oscillator strengths, resulting from the circumstellar absorption from neutral metals over the *k* line (Luttermoser 1996, 2000). Meanwhile, non-Mira red giant stars typically show the *k* line being stronger than the *h* line in accordance with their respective oscillator strengths (Robinson & Carpenter 1995). The Mg II *k* to *h* emission from Mira B more closely follows the relative strength of *k* and *h* as seen in the non-Mira red giants than in single Mira-type red giants.

2. DESCRIPTION OF OBSERVATIONS

We present *IUE* observations taken between 1979 and 1995. Some of these data were presented by Reimers & Cassatella (1985). The LWP and LWR cameras were used at high resolution (0.2 Å), which covers the range of wavelengths from 1800 Å to 3200 Å. For details of the instrument, see Boggess et al. (1978a,

Table 1
High Resolution Observations for Mira AB

Row	Image ID	Dispersion	Aperture	Obs. Date	Exposure Time (s)	Phase
1	LWR05869	High	Large	1979 Oct 18	6600	0.97
2	LWP18359	High	Large	1990 Jul 12	7200	0.78
3	LWP18599	High	Large	1990 Aug 16	4200	0.89
4	LWP19714	High	Large	1991 Feb 7	1320	0.51
5	LWP19716	High	Large	1991 Feb 7	1080	0.51
6	LWP22347	High	Large	1992 Feb 6	1500	0.37
7	LWP22349	High	Large	1992 Feb 6	3000	0.37
8	LWP29171	High	Large	1994 Sep 13	1500	0.41
9	LWP29172	High	Large	1994 Sep 13	3000	0.41
10	LWP29227	High	Large	1994 Sep 23	2400	0.59
11	LWP29623	High	Large	1994 Dec 3	3700	0.61
12	LWP29684	High	Large	1994 Dec 11	3000	0.64
13	LWP29784	High	Large	1994 Dec 29	3600	0.69
14	LWP29795	High	Large	1994 Dec 30	3900	0.70
15	LWP29961	High	Large	1995 Dec 12	3000	0.83

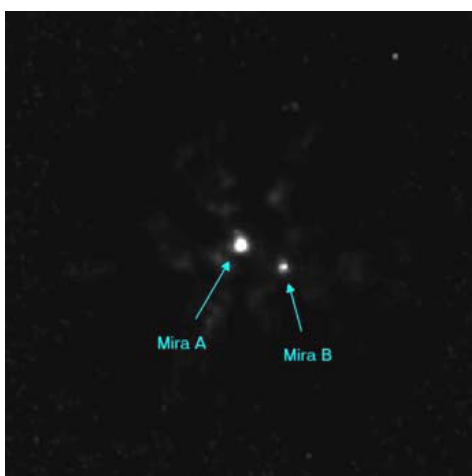


Figure 1. First image to resolve Mira B, taken with the *HST*'s Wide Field and Planetary Camera, with an $H\beta$ filter. (Credit M. Bobrowsky and NASA).

(A color version of this figure is available in the online journal.)

1978b). The *IUE* data sets are listed in Table 1, including the image, resolution, aperture, observation date, exposure time, and phase of each observation. We note that in this long wavelength range, there are broad collisionally excited lines and Mg II *k* and *h* emission lines at 2800 Å primarily arising from Mira B. The data were analyzed by the MIDAS software, and we calculated the line flux, line width, and the errors associated with them.

3. Mg II *k* AND *h* EMISSION LINES

3.1. Lines at 2800 Å

The magnesium lines are broad emission lines at 2795.528 Å (*k* line) and at 2802.705 Å (*h* line) resulting from collisional excitation (Luttermoser 2000), probably arising from Mira B. Figures 2–5 show the profiles of these lines at different phases, and how these profiles change both in shape and in flux with phase. Wood & Karovska (2000) have studied some single Mira variables (S Car, R Car, L² Pup, T Cep, and R Leo) and concentrated on Mg II *k* and *h* lines. In their study, they mentioned that the Mg II lines are blueshifted and disappear

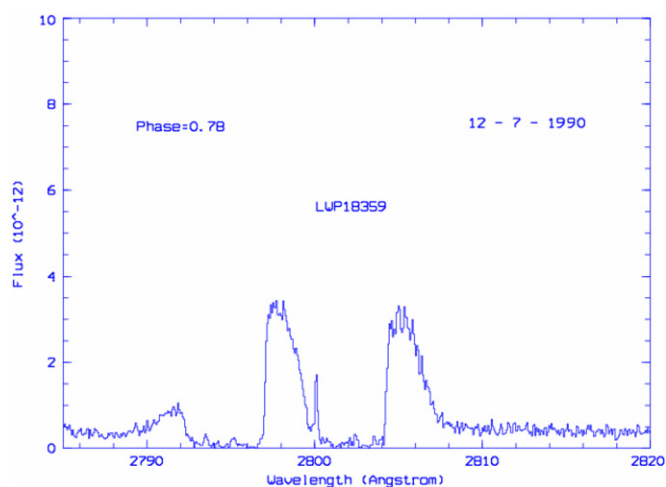


Figure 2. *IUE* Spectrum of Mg II *h* and *k* emission lines at phase 0.78. Note that the flux is plotted in units of $\text{erg s}^{-1} \text{cm}^{-2} \text{Å}^{-1}$.

(A color version of this figure is available in the online journal.)

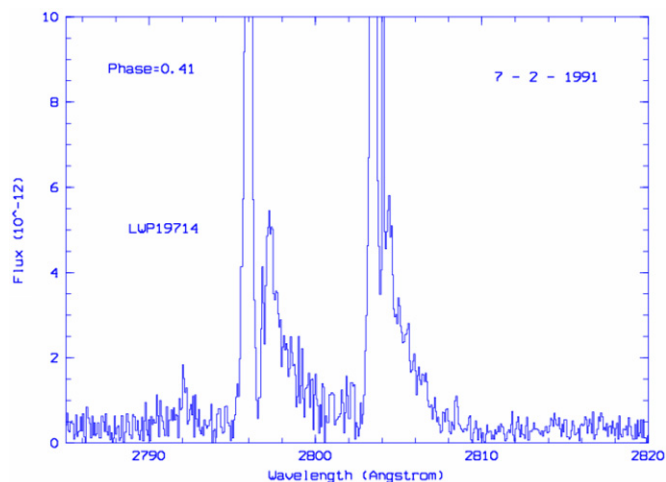


Figure 3. *IUE* Spectrum of Mg II *h* and *k* emission lines at phase 0.41. Note that the flux is plotted in units of $\text{erg s}^{-1} \text{cm}^{-2} \text{Å}^{-1}$.

(A color version of this figure is available in the online journal.)

at some phases, but these lines in our case are redshifted and always exist in all phases but with varying fluxes.

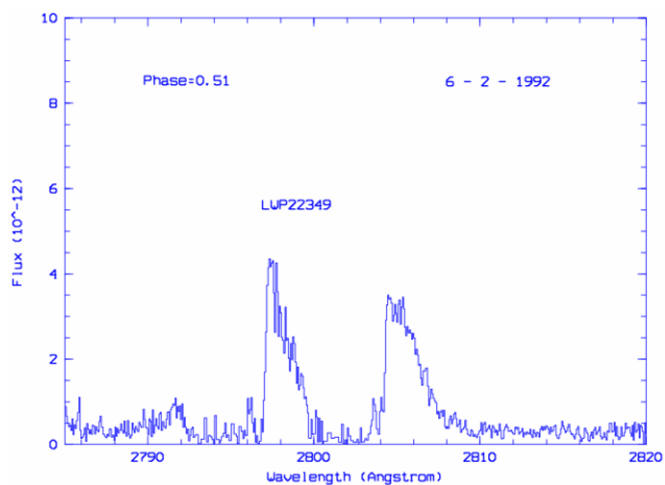


Figure 4. IUE Spectrum of Mg II *h* and *k* emission lines at phase 0.51. Note that the flux is plotted in units of $\text{erg s}^{-1} \text{cm}^{-2} \text{\AA}^{-1}$.

(A color version of this figure is available in the online journal.)

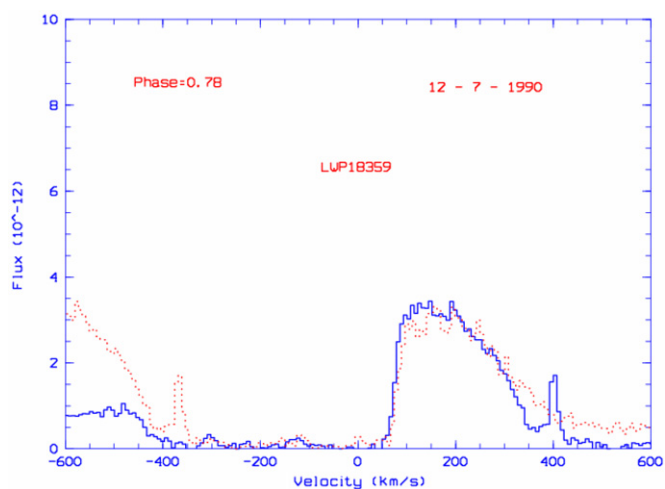


Figure 6. IUE observations of the Mg II *h* and *k* profiles in velocity units at phase 0.78. Note that the flux is plotted in units of $\text{erg s}^{-1} \text{cm}^{-2} \text{\AA}^{-1}$.

(A color version of this figure is available in the online journal.)

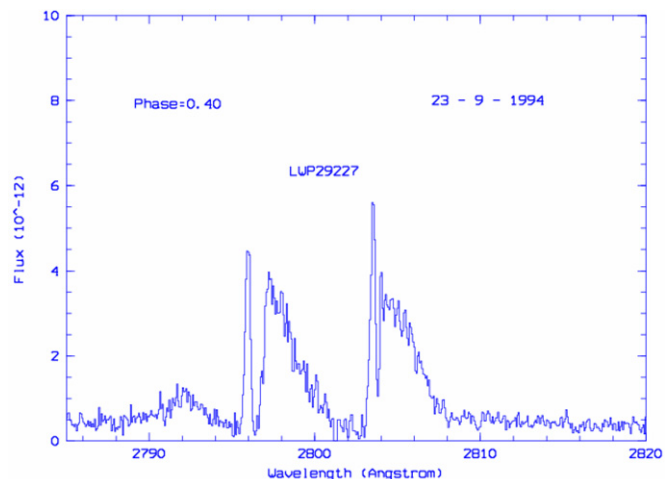


Figure 5. IUE Spectrum of Mg II *h* and *k* emission lines at phase 0.40. Note that the flux is plotted in units of $\text{erg s}^{-1} \text{cm}^{-2} \text{\AA}^{-1}$.

(A color version of this figure is available in the online journal.)

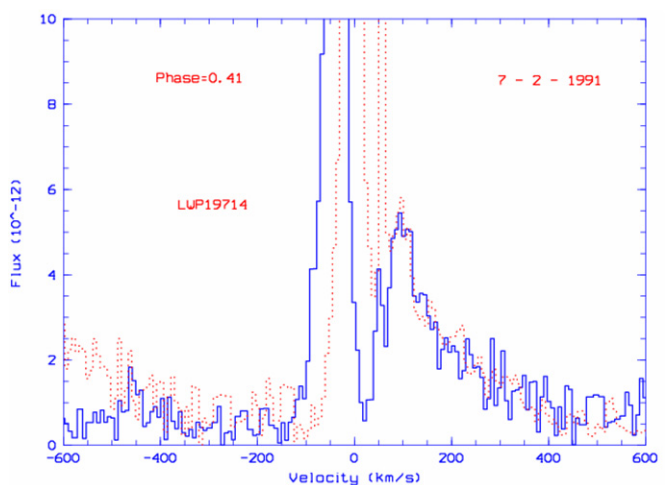


Figure 7. IUE observations of the Mg II *h* and *k* profiles in velocity units at phase 0.41. Note that the flux is plotted in units of $\text{erg s}^{-1} \text{cm}^{-2} \text{\AA}^{-1}$.

(A color version of this figure is available in the online journal.)

3.2. Emission Lines in Velocity Units

In Figures 6–9, we display the observed Mg II *k* and *h* line profiles plotted with velocity units. The *k* line is shown as a solid line and the *h* line is represented by a dotted line. The date, time, and phase of each observation are indicated in the figures, and from these plots we deduce the following.

1. The broad emission profile in Mg II extends up to 500 km s^{-1} and is redshifted, as shown in the figures.
2. Figures 6 and 8 display additional overlying absorption on the extreme red side of the *k* line as compared with the *h* line. When overplotting the *k* and *h* lines in velocity units, there is evidence that the extreme blue-side emission of the *h* line is coincident with the red-side emission of the *k* line; hence they are blended. The overlying wind absorption of the blue side of the *h* line, which extends out to -450 km s^{-1} from the line center and partially obscures the extreme red-side emission of the *k* line starting at around $+300 \text{ km s}^{-1}$. The fact that this additional *k*-line extreme red side absorption is not seen in all of the observations suggests

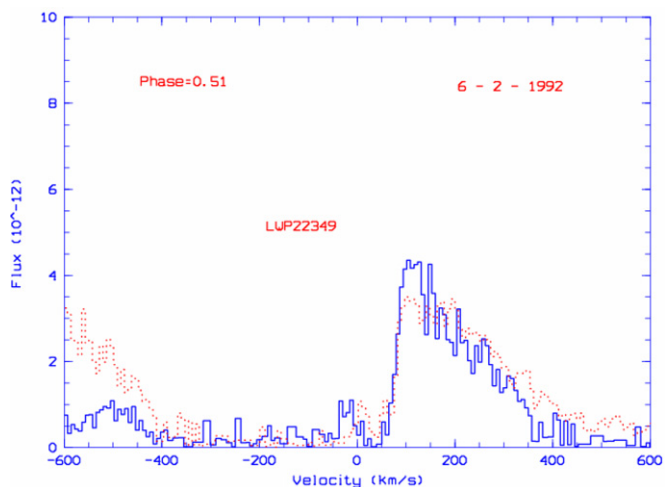


Figure 8. IUE observations of the Mg II *h* and *k* profiles in velocity units at phase 0.51. Note that the flux is plotted in units of $\text{erg s}^{-1} \text{cm}^{-2} \text{\AA}^{-1}$.

(A color version of this figure is available in the online journal.)

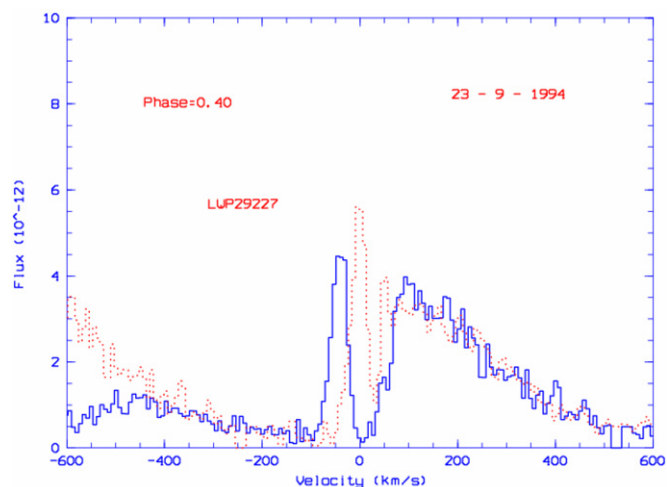


Figure 9. IUE observations of the Mg II *h* and *k* profiles in velocity units at phase 0.40. Note that the flux is plotted in units of $\text{erg s}^{-1} \text{cm}^{-2} \text{\AA}^{-1}$.

(A color version of this figure is available in the online journal.)

that the opacity of Mg II in the wind of Mira B varies over time. A likely reason for this is a change in density of the wind over time, as has been recently suggested by Wood & Karovska (2006).

3. On the blue side of the Mg II line, there are low-velocity emission and absorption components, the absorption components being due to interstellar and circumstellar shells around the two stars, while the sharp emission—from Mira A, and very strong at phases 0.40 and 0.41—is superposed upon the broad emission and wind profiles from Mira B.

4. CORRELATIONS BETWEEN LINE PARAMETERS AND PHASE

4.1. Short- and Long-Period Relations for the Mg II *k* Line

4.1.1. The Relation Between the Line Flux and Phase

Figure 10 shows the relation between the line flux and phase of Mira A in a short period in 1994. As can be seen in this figure, the values of fluxes vary at different phases between high and low values. The reasons for this are as follows: Mira A ejects much of its mass in the form of a stellar wind. Some of this material is gravitationally captured by the companion, Mira B, creating an accretion disk. Both the companion and disk affect each other mutually, and this can be seen in their spectrum. The mass transfer between the two stars increases and decreases at different phases. So when the density is high, the probability for the transition being available for the emission of Mg II lines is high, which explains the high values of flux at some phases; by contrast when the density is low, the probability for this transition is low, which explains the low values of flux at other phases. In short, the density of accreted matter differs at different phases. In addition to this, Mira A is at its brightest at low phases (0.1–0.3), when it is at its smallest size and highest effective temperature. The interpretation is that the high values of fluxes at low phases occur because of the increasing temperature. At phases between 0.5 and 0.9, Mira A is at its dimmest, when it is at its largest size and coolest effective temperatures, consistent with the low values of fluxes at these phases, as seen in Figures 10 and 11. For a single Mira variable, Wood & Karovska (2000) revealed that the Mg II fluxes vary from one cycle to

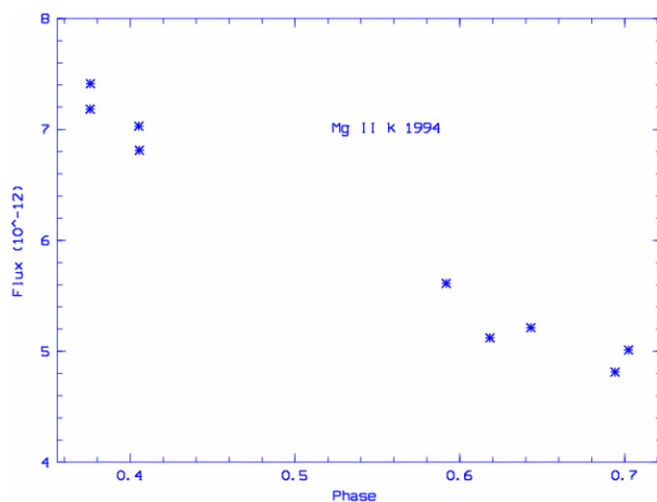


Figure 10. Mg II *k* line flux with phase in short period 1994. Note that the integrated flux is plotted in units of $\text{erg s}^{-1} \text{cm}^{-2} \text{\AA}^{-1}$.

(A color version of this figure is available in the online journal.)

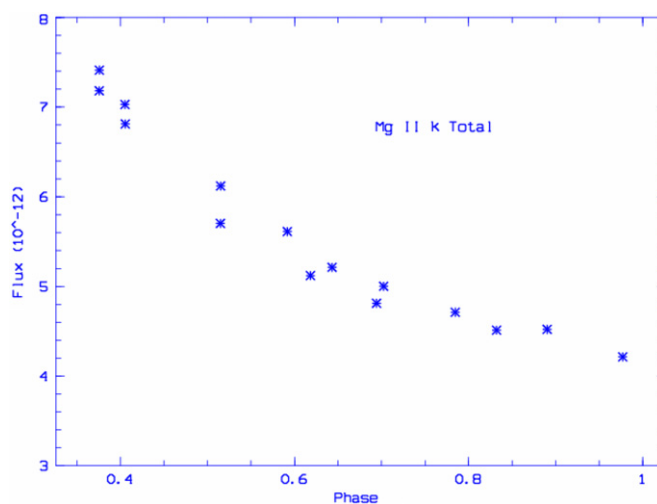


Figure 11. Mg II *k* line flux with phase in long period 1979–1995. Note that the flux is plotted in units of $\text{erg s}^{-1} \text{cm}^{-2}$.

(A color version of this figure is available in the online journal.)

the next for R Car. Figure 11 shows the relation between the line flux and phase during the long period between 1979 and 1995, which is consistent with the previous interpretation. The uncertainty in the values of the flux was determined using the procedures outlined by Lenz & Ayers (1992) and F. Bruhweiler (2002, private communication).

4.1.2. Gaussian Fitting of Broad Mg II Emission Lines

By looking at Figures 6–9, there are three main spectral features: (1) Broad Mg II emission lines (*k* and *h*) from Mira B, (2) Narrow emission peaks from Mira A, and (3) Absorption features from circumstellar material and Mira B's wind.

Consequently, the blue sides of Mg II emission lines are suppressed by absorption from Mira B's wind. To calculate the widths of these emission lines, we performed Gaussian fitting, which included these spectral features (see Figure 12). This is based on fitting the observed portions of the emission line wings with a Gaussian function, letting the wavelength boundaries of the violet and red wings to be fitted by λ_1 to λ_2 and λ_3 to λ_4 , respectively. After subtraction of the local continuum and

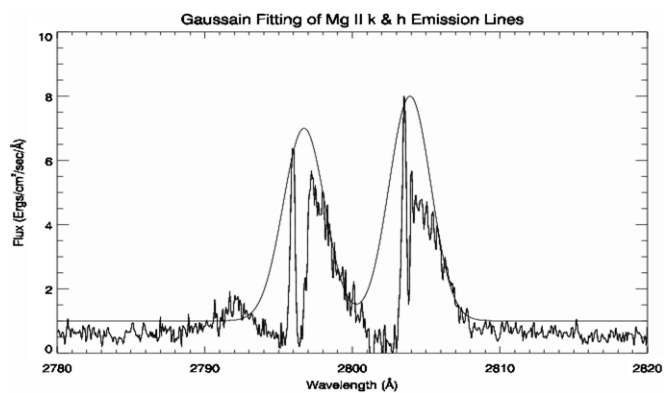


Figure 12. Gaussian fitting of Mg II *k* and *h* emission lines.

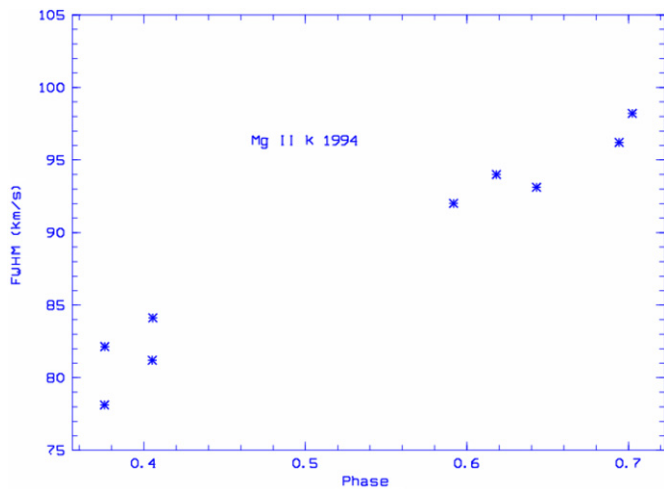


Figure 13. Mg II *k* line width with phase in short period 1994.
(A color version of this figure is available in the online journal.)

normalization to the line peak emission, all spectra were fitted with a Gaussian function. In this case, line widths were defined as the full width of the fitted profile measured at half maximum of the observed line peak.

4.1.3. The Relation Between the Line Width and Phase

Figure 13 shows the relation between the line width and phase. Our method of measurements for line widths depends on taking into account the effect of wind absorption. The Mg II *k* and *h* line profiles often appear asymmetric to some extent, with the red side affected by wind absorption. Nevertheless, the profiles can be represented reasonably as a Gaussian and can, therefore, be quantified with Gaussian fits. It is known that any spectral line has constant natural width, but in Figure 12, the line width varies at different phases because of the changing density of matter around the hot companion, that is, with high density, there is greater collisional broadening. Figure 14 shows the relation between the line width and phase in the long period between 1979 and 1995, which is consistent with the previous interpretation. For a single Mira variable, Wood & Karovska (2000) revealed that there is a possible correlation between the pulsation period and line width. The uncertainty for the values of the width is in the range between 0.06 Å and 0.11 Å, by using the procedures outlined by Lenz & Ayres (1992).

4.1.4. The Relation Between the Line Velocity and Phase

Figure 15 shows the relation between the line velocity and phase; that is, showing the behavior of the velocity of these

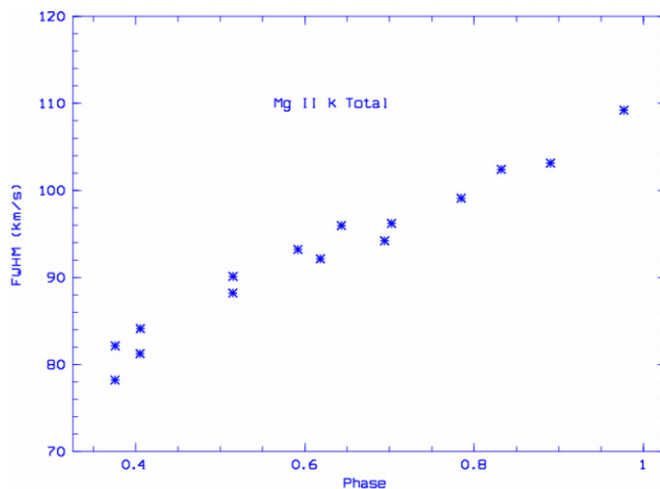


Figure 14. Mg II *k* line width with phase in long period 1979–1995.
(A color version of this figure is available in the online journal.)

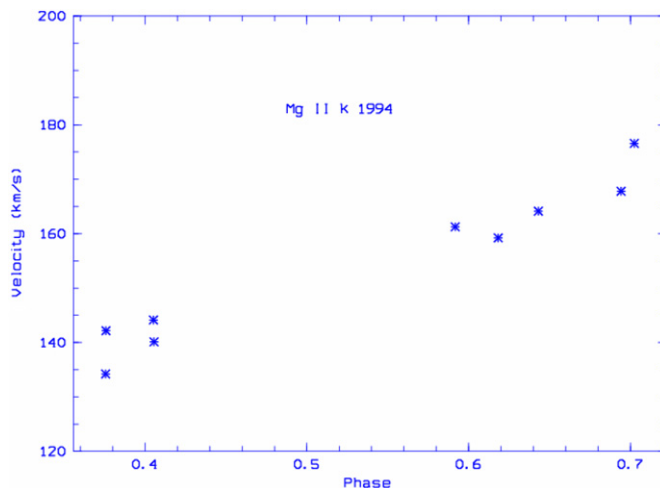


Figure 15. Mg II *k* line velocity with phase in short period 1994.
(A color version of this figure is available in the online journal.)

lines at different times. At low phases; that is, the contraction phases of Mira A between 0.1 and 0.3, the velocity of atoms and consequently the velocity of the environment as a whole are small, consistent with the low values of the line velocities at these phases, while at expansion phases (0.5–0.9), the velocity of atoms is high, consistent with the high values of velocities at these phases seen in Figures 15 and 16. Figure 16 shows the relation between the line velocity and phase in the long period between 1979 and 1995, which is consistent with the previous interpretation. For a single Mira variable, Wood & Karovska (2000) also demonstrated a correlation between the line velocity and phase.

4.2. Short- and Long-Period Relations for the Mg II *h* Line

4.2.1. The Relation Among the Line Flux, Line Velocity, and Phase

Figures 17 and 18 show the relations among the line flux, line velocity, and phase, which are also consistent with the previous interpretation of the Mg II *k* line concerning the increasing and decreasing density around the hot companion. Figures 19 and 20 show the relation among the line flux, line velocity, and phase, but in the long period between 1979 and 1995.

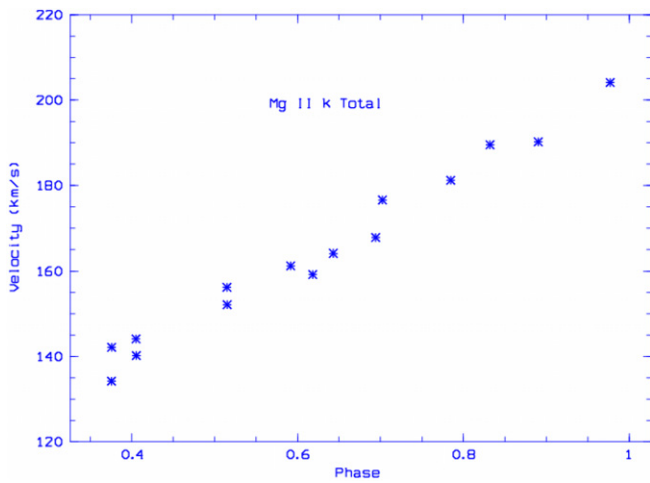


Figure 16. Mg II *k* line velocity with phase in long period of 1979–1995. (A color version of this figure is available in the online journal.)

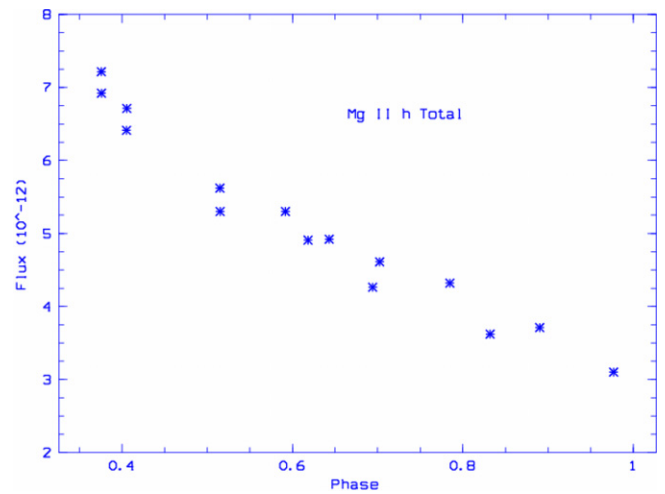


Figure 19. Mg II *h* line flux with phase in the long period 1979–1995. Note that the flux is plotted in units of $\text{erg s}^{-1} \text{cm}^{-2}$. (A color version of this figure is available in the online journal.)

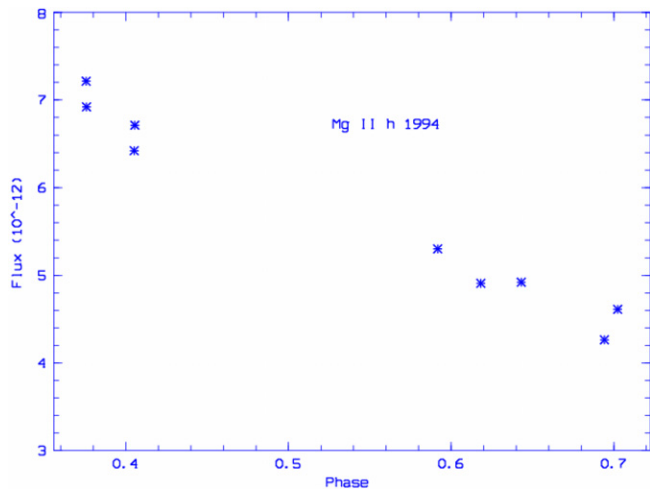


Figure 17. Mg II *h* line flux with phase in short period 1994. Note that the flux is plotted in units of $\text{erg s}^{-1} \text{cm}^{-2}$. (A color version of this figure is available in the online journal.)

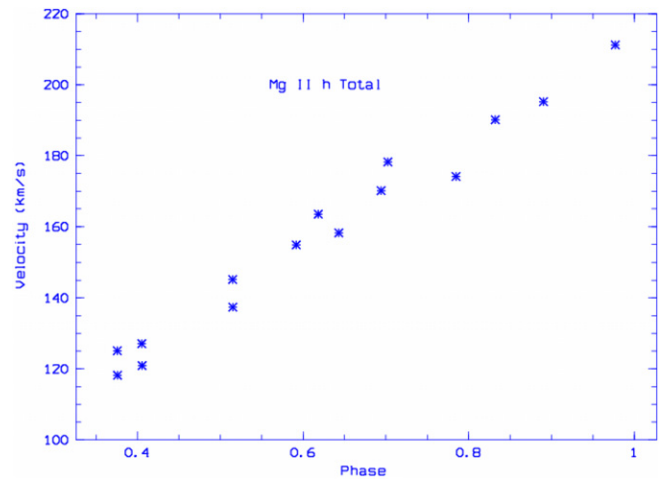


Figure 20. Mg II *h* line velocity with phase in the long period 1979–1995. (A color version of this figure is available in the online journal.)

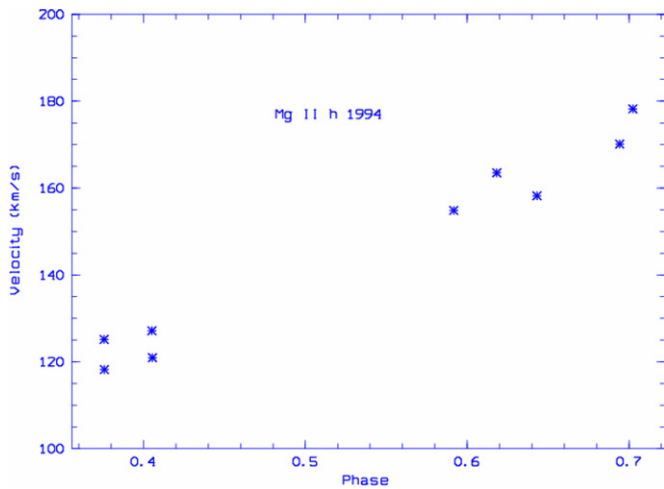


Figure 18. Mg II *h* line velocity with phase in the short period 1994. (A color version of this figure is available in the online journal.)

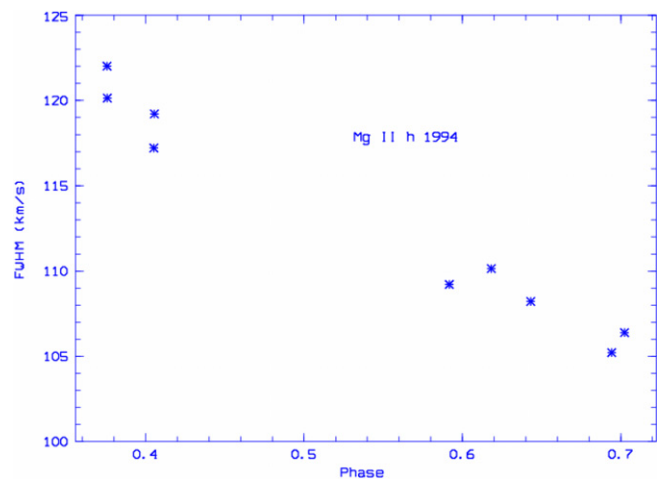


Figure 21. Mg II *h* line width with phase in the short period 1994. (A color version of this figure is available in the online journal.)

4.2.2. The Relation Between the Line Width and Phase

Figure 21 shows the relation between the line width and phase. These data are also consistent with the previous interpretation

of changing density and its subsequent effect on the width of the line. Figure 22 shows the data for the long period from 1979 to 1995. Note that both the *k* and *h* lines behave inversely with

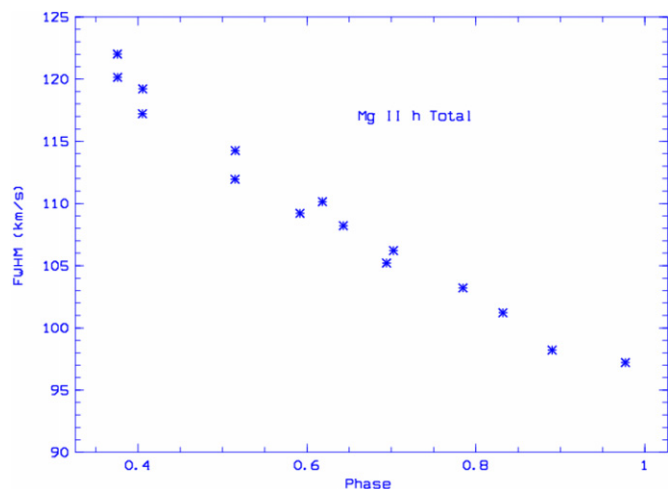


Figure 22. Mg II *h* line width with phase in the long period 1979–1995.

(A color version of this figure is available in the online journal.)

Table 2

The Line Flux of Both Mg II *h* and Mg II *k* Emission Lines and the Ratio Between Them

<i>k</i> Line Flux	<i>h</i> Line Flux	<i>k/h</i> Ratio	Phase
4.21521E-012	3.10211E-012	1.35	0.97
4.71214E-012	4.32012E-012	1.09	0.78
4.52101E-012	3.71201E-012	1.21	0.89
5.70341E-012	5.62101E-012	1.01	0.51
6.12014E-012	5.30124E-012	1.15	0.51
7.18246E-012	7.21404E-012	0.99	0.37
7.41241E-012	6.92104E-012	1.07	0.37
7.02965E-012	6.41201E-012	1.09	0.41
6.81241E-012	6.71204E-012	1.01	0.41
5.61211E-012	5.30121E-012	1.05	0.59
5.12121E-012	4.90884E-012	1.04	0.61
5.21312E-012	4.92145E-012	1.05	0.64
4.81231E-012	4.26403E-012	1.12	0.69
5.00124E-012	4.61201E-012	1.08	0.70
4.51212E-012	3.62141E-012	1.24	0.83

each other, as seen in Figures 14 and 22. This may be the result of the stellar wind causing absorption of the *k* line.

5. THE PHYSICAL MEANING OF THE OBSERVED RATIO OF Mg II *k* TO *h* LINES

Table 2 contains fluxes for both the *k* and *h* lines with their corresponding ratios. We note that in general, the flux of the *k* line is greater than the flux of the *h* line. This can be explained by the optical depth of the *k* line being twice that of the *h* line due to the factor of 2 difference in its oscillator strength (which is, of course, due to the factor of 2 difference in their statistical weights). The odd value where $h > k$ may be related to pulsation effects which, at certain times, have an inverse effect on both *h* and *k* lines. The most important statistic from Table 2 is the fact that the $f(k)/f(h)$ ratio is largest near phases 0.83, 0.89, and 0.97, and smallest near phase 0.40, since Mira A's peak Mg II flux will occur around phase 0.4 and not be detectable with IUE from approximately phase 0.7 through phase 0.1. Since $f(k)/f(h) < 1$ in single Miras due to overlying absorption on the *k* line from circumstellar neutral metal lines, the Mg II flux from Mira A forces this ratio close to unity at these phases. For the Mira variables S Car and R Car, Bookbinder et al. (1989) showed that the *h* line is significantly stronger than the *k* line.

6. CONCLUSION

We have analyzed IUE observations of Mira AB for the period from 1979 to 1995 with regard to the variations of flux, width, and velocity of the Mg II *k* and *h* emission lines at different times. From this study, we found that the velocities of the Mg II *k* and *h* lines extend out to 500 km s⁻¹ (in velocity units). There is evidence that extreme blue-side emission of the *h* line is coincident with the red-side emission of the *k* line; hence, there is blending of this important doublet. The overlying wind absorption of the blue side of the *h* line, which extends out to -450 km s⁻¹ from the line center, partially obscures the extreme red side of the *k* line. There are low-velocity absorption and emission components in the blue side of the Mg II lines, the absorption component being due to interstellar and circumstellar shells around the two stars, while the sharp emission is from Mira A. The density of accreted matter around Mira B changes as a result of both the quantity of ejected matter and the ability of the hot companion to attract the mass, depending on the changes in distance to Mira A between its contraction and expansion phases. The density at some phases is high, which leads to increased flux, width, and velocity, while at other phases the density is low, which leads to decreased flux, width, and velocity. Mg II emission in single Mira variables often displays a stronger *h* line than *k* line (Bookbinder et al. 1989), opposite to the values of their oscillator strengths, resulting from circumstellar absorption from neutral metals over the *k* line (Luttermoser 1996, 2000). Meanwhile, non-Mira red giant stars typically show the *k* line being stronger than the *h* line in accordance with their respective oscillator strengths (Robinson & Carpenter 1995). The Mg II *k* to *h* emission from Mira B more closely follows the relative strength of *k* and *h* as seen in the non-Mira red giants than in single Mira-type red giants.

M.R.S. thanks P. Bonifacio for providing the programs used in data analysis and reduction. He also expresses his great thanks to Professor F. Bruhweiler for his productive guidance and continuous support and scientific assistance. He also thanks Professor E. Sion for his useful discussions and important comments. M.B. acknowledges support for this work from NASA, through grant number HST-AR-10304.01-A from the Space Telescope Science Institute, which is operated by the Association of Universities for Research in Astronomy, Inc., under NASA contract NAS5-26555. Finally, the authors would also like to thank the anonymous referee for all the useful suggestions made to improve this paper.

REFERENCES

- Boggess, A., et al. 1978a, *Nature*, 275, 372
 Boggess, A., et al. 1978b, *Nature*, 275, 377
 Bookbinder, J. A., Brugel, E. W., & Brown, A. 1989, *ApJ*, 342, 56
 Brugel, E. W., Willson, L. A., & Candmos, R. 1986, in ESA SP 263, New Insights in Astrophysics: Eight Years of UV Astronomy with IUE (Nordwijk: ESA), 213
 Deuch, A. J. 1960, in Stellar Atmospheres 6, Stars and Stellar Systems, ed. J. L. Greenstein (Chicago, IL: Univ. Chicago Press), 543
 Joy, A. H. 1954, *ApJ*, 1, 58
 Jura, M., & Helfand, D. J. 1984, *ApJ*, 287, 785
 Karovska, M., Hack, W., Raymond, R., & Guinan, E. 1997, *ApJ*, 482, L175
 Lenz, D. D., & Ayers, T. R. 1992, *PASP*, 104, 1104
 Luttermoser, D. G. 1996, in ASP Conf. Ser. 109, Cool Stars, Stellar Systems and the Sun, Ninth Workshop, ed. R. Pallavicini & A. K. Dupree (San Francisco, CA: ASP), 535
 Luttermoser, D. G. 2000, *ApJ*, 536, 923L
 Perryman, M. A. C., et al. 1997, *A&A*, 323, L49
 Reimers, D., & Cassatella, A. 1985, *ApJ*, 297, 275

- Robinson, R. D., & Carpenter, K. G. 1995, *ApJ*, **442**, 328
Sutton, E. C., Stary, J. W. V., & Towness, C. H. 1978, *ApJ*, **230**, L105
Wannier, P. G., Redman, R. O., Philips, T. G., Leighton, R. B., Knapp, G. R., & Huggins, P. J. 1980, in IAU Symposium 87, *Interstellar Molecules*, ed. B. H. Andrews (Dordrecht: Reidel), 487
- Warner, B. 1972, *MNRAS*, **159**, 95
Wood, B. E., & Karovska, M. 2000, *ApJ*, **535**, 304
Wood, B. E., & Karovska, M. 2006, *ApJ*, **649**, 410
Yamashita, Y., & Maehara, H. 1977, *PASJ*, **29**, 319
Yamashita, Y., & Maehara, H. 1978, *PASJ*, **30**, 409